Tailoring higher-order topological phases via orbital hybridization

Maxim Mazanov [*] and Maxim A. Gorlach [†]
School of Physics and Engineering, ITMO University, St. Petersburg 197101, Russia

(Received 3 November 2021; revised 1 April 2022; accepted 13 April 2022; published 13 May 2022)

Higher-order topological insulators (HOTIs) have attracted much attention in photonics due to the tightly localized disorder-robust corner and hinge states. Here, we reveal an unconventional HOTI phase with vanishing dipole and quadrupole polarizations. This phase arises in the array of evanescently coupled waveguides hosting degenerate s- and d-type orbital modes arranged in a square lattice with four waveguides in the unit cell. As we prove, the degeneracy of the modes with the different symmetry gives rise to the nontrivial topological properties rendering the system topologically equivalent to the two copies of the anisotropic two-dimensional Su-Schrieffer-Heeger model rotated by 90° with respect to each other and based on $s \pm d$ hybridized orbitals. We probe the unusual topology of the model by constructing a quantized Fu-Kane-type pseudospin pump. Our results introduce a route to tailor higher-order band topology leveraging both crystalline symmetries and accidental degeneracies of the different orbital modes.

DOI: 10.1103/PhysRevB.105.205117

Introduction. Higher-order topological insulators (HOTIs) are unusual states of matter hosting topologically protected localized states of at least two dimensions less than the system itself [1,2]. The understanding of their physics relies either on nontrivial bulk dipole polarization [3] or higher-order multipole polarization [4,5] associated with the Bloch bands and giving rise to the quantized corner charges. This characterization is also valid for spinful and spin-orbit coupled systems [6]. Recent photonic realizations are exploiting suitably designed lattices [7,8], intentionally tailored negative effective couplings, or artificial gauge fields [9–11], and the entire area continues to rapidly evolve [2]. In these approaches, lattice symmetry and the engineered couplings between the elementary building blocks play the key role ensuring the nontrivial topology of the bands.

In this paper, we take another route to higher-order topology exploiting multimode constituent elements and harnessing *both* lattice geometry and accidental degeneracy of the different orbital modes. Previously, the concept of orbital hybridization has been used to tailor the dispersion inducing such features as Dirac cones and flat bands [12,13] or manipulate couplings between the elements by hybridizing either s- and p-type modes with the different inversion parities [14–19] or p_x and p_y modes corresponding to the different polarization states [20–24].

In contrast, here we harness the idea of orbital hybridization to construct an unconventional HOTI phase arising in a square waveguide lattice with four sites in the unit cell [Fig. 1(a)] resembling the two-dimensional Su-Schrieffer-Heeger model (2D SSH) [25–28]. While in the single-orbital limit this model does not have a zero-energy band gap, the interference of the degenerate monopolar (s-like) and quadrupolar (d-like) modes at each site gives rise to the complete band gap hosting disorder-robust midgap corner states.

Unlike previous realizations of higher-order topology, our system is characterized by vanishing dipole and quadrupole polarizations. Despite that, we reveal the nontrivial nature of the model by showing its topological equivalence to the direct sum of two anisotropic 2D SSH models for $s + d$ and $s - d$ hybrid orbitals. The effective anisotropy of the coupling for $s \pm d$ orbitals is induced via the generalized near-field Kerker effect [29,30]. In turn, each of the hybrid orbitals treated as a distinct pseudospin is topologically nontrivial giving rise to the topological corner states. Vanishing conventional invariants along with the orbital degree of freedom suggest a deep analogy of our system to the quantum spin Hall effect (QSHE). While the latter is characterized by the spin Chern number in the decoupled spin limit [31], in our case the topology may be characterized by the respective higher-order analog.

It should be also stressed that our system is different from the celebrated spinful $s - d$-hybridized model of quadrupole insulator reported in condensed matter physics [32]. Contrary to that model relying on spin-orbit coupling, we introduce here geometric gap-opening terms which enable higher-order topology readily attainable in waveguide lattices. Furthermore, our proposal is also different from the recent works Refs. [33,34]. In Ref. [33], each topological corner state in a hexagonal sample has a well-defined pseudospin that couples to the respective pseudospin-polarized edge state, while Ref. [34] introduces corner states in coupled QSH exciton bilayers under applied interlayer voltage bias and external magnetic field. In both cases, each corner hosts no more than one corner state, and higher-order topology matches one of the conventional classes [3] in contrast to our proposal.

Model and band structure. We consider a square lattice of two-mode waveguides depicted in Fig. 1(a); each of the waveguides hosts two modes having the same propagation

[*] maxim.mazanov@metalab.ifmo.ru
[†] m.gorlach@metalab.ifmo.ru

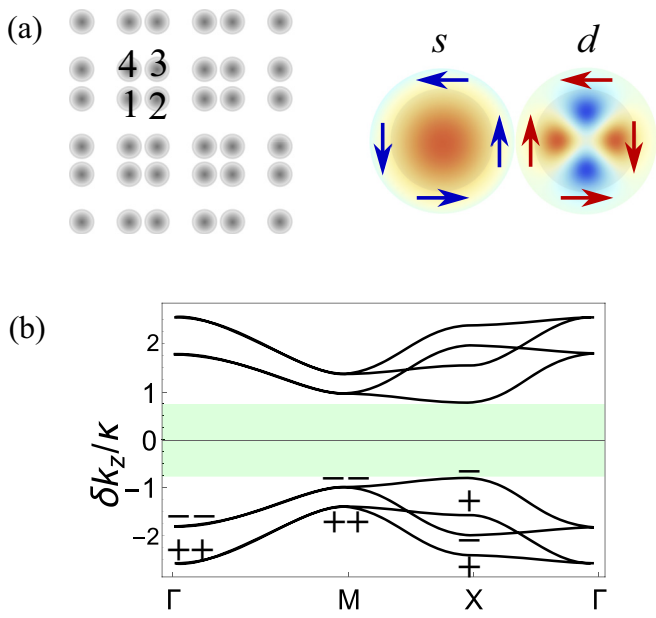

FIG. 1. (a) Two-dimensional Su-Schrieffer-Heeger lattice with degenerate monopolar (TE_{0m}; left) and quadrupolar (HE_{2k}; right) modes at each site. Arrows indicate the direction of electric field in the respective modes. (b) Bulk band structure with a complete gap highlighted by green; ± signs indicate inversion eigenvalues at high-symmetry points. The calculation is performed for $\kappa = \gamma$, $\Delta = 0.7\kappa$, $\alpha = 0.3$.

constants in the chosen frequency range. s and d orbital modes correspond to TE_{0m}/TM_{0n} and HE_{2k} waveguide modes with arbitrary radial indices m, n, k, respectively, and typical field profiles sketched in Fig. 1(a).

The described model possesses C_2 rotational symmetry as well as inversion symmetry. Note that although the quadrupolar mode is doubly degenerate, its 45°-rotated partner does not contribute to the effective photonic Hamiltonian since its electric field has zero overlaps with the monopolar modes in the nearest-neighbor waveguides. However, triple degeneracy of TE_{0m}/TM_{0n}, and $2 \times HE_{2k}$ orbitals will yield two noninteracting copies of our model.

Assuming the interaction of the nearest neighbors, we obtain the set of coupled-mode equations for the described two-mode lattice model [35]:

$$-i\frac{d}{dz}\begin{pmatrix} u \\ v \end{pmatrix}_{m,n} = \hat{\kappa}_-\left[\begin{pmatrix} u \\ v \end{pmatrix}_{m-1,n} + \begin{pmatrix} u \\ v \end{pmatrix}_{m+1,n}\right] + \hat{\kappa}_+\left[\begin{pmatrix} u \\ v \end{pmatrix}_{m,n-1} + \begin{pmatrix} u \\ v \end{pmatrix}_{m,n+1}\right], \quad (1)$$

where z is the coordinate along the waveguide axes, m and n are horizontal and vertical unit cell indices, respectively, while u and v denote the amplitudes of the first (monopolar) and the second (quadrupolar) modes in each waveguide. Due to the coupling between the waveguides, these amplitudes depend on z. In such setting, the problem of mode evolution with z coordinate is fully analogous to the problem of temporal evolution in the Schrödinger equation with the same tight-binding Hamiltonian. Due to that, we inspect the dependence $\delta k_z(k_x, k_y)$ instead of $\omega(k_x, k_y)$ [36,37], where δk_z is the difference of propagation constants in the array and in a single isolated waveguide.

Symmetries of the mode profiles result in the coupling matrices: $\hat{\kappa}_\pm = \begin{pmatrix} \kappa & \pm i\Delta \\ \mp i\Delta & \gamma \end{pmatrix}$, where κ, γ, Δ are real-valued positive coupling integrals quantifying the interaction of the mode pairs u, u (κ), u, v ($\pm i\Delta$), and v, v (γ) [35].

Next, we incorporate geometric shrinking-expanding lattice distortions into our model [Fig. 1(a)]. For simplicity, we approximate the effect of such distortion by the single scalar parameter $0 \leqslant \alpha \leqslant 1$ that changes all the couplings proportionally, $\hat{\kappa}_\pm \to \alpha\hat{\kappa}_\pm$. Choosing the numbering of sites consistent with Fig. 1(a), we recover the 8×8 Bloch Hamiltonian

$$\hat{H}(\mathbf{k}) = \begin{pmatrix} 0 & \beta_x^*\hat{\kappa}_- & 0 & \beta_y^*\hat{\kappa}_+ \\ \beta_x\hat{\kappa}_- & 0 & \beta_y^*\hat{\kappa}_+ & 0 \\ 0 & \beta_y\hat{\kappa}_+ & 0 & \beta_x\hat{\kappa}_- \\ \beta_y\hat{\kappa}_+ & 0 & \beta_x^*\hat{\kappa}_- & 0 \end{pmatrix}, \quad (2)$$

where $\beta_{x,y} \equiv \alpha e^{ik_{x,y}} + 1$. Even though α should be generally regarded as a matrix with norm $||\hat{\alpha}|| < 1$, this simplified model already captures the topological origin of our system predicting topological corner states in agreement with the full-wave numerical simulations discussed below.

The Bloch modes of the system are found as the solutions to the eigenvalue equation of the form $\hat{H}(\mathbf{k})(\mathbf{v}_1, \mathbf{v}_2, \mathbf{v}_3, \mathbf{v}_4)^T = \delta k_z(\mathbf{v}_1, \mathbf{v}_2, \mathbf{v}_3, \mathbf{v}_4)^T$, where $\mathbf{v}_i = (u_i, v_i)^T$, and δk_z is an unknown eigenvalue.

The calculated band diagram for $\hat{H}(\mathbf{k})$ with $\alpha < 1$ is shown in Fig. 1(b). We observe that the 2D SSH-type distortions open a complete gap between the two sets of bands. In the special case $\Delta = \kappa = \gamma$, the bands become pairwise degenerate.

Higher-order topology. To assess the topological nature of our model, we first note that it possesses two commuting reflection symmetries M_x and M_y [35], which rules out higher-order quadrupolar topology since the bulk Wannier bands are then necessarily gapless [4,5].

Next, we test whether our model is a higher-order topological crystalline insulator by calculating symmetry indicators at high-symmetry points of the Brillouin zone [3]. In this way, we find that the conventional HOTI index $\chi^{(2)}$ vanishes [35].

On the other hand, in the special case $\kappa = \gamma$, the Hamiltonian Eq. (2) can be transformed to the following block-diagonal form:

$$\hat{H}' \equiv \hat{U}^\dagger\hat{H}\hat{U} = \begin{pmatrix} \hat{h}(k_x, k_y) & 0 \\ 0 & \hat{h}(k_y, -k_x) \end{pmatrix} \quad (3)$$

with the basis formed by $s + d$ orbitals for the upper diagonal block, and by $s - d$ orbitals for the lower block [35]. The matrix block $\hat{h}(k_x, k_y)$ in Eq. (3) represents the anisotropic 2D SSH model with real couplings $\kappa + \Delta$, $\alpha(\kappa + \Delta)$ along x, and $\kappa - \Delta$, $\alpha(\kappa - \Delta)$ along y; see Fig. 2. When $\alpha < 1$ and $\Delta \neq \kappa$, such anisotropic 2D SSH model is a well-known C_2-symmetric higher-order topological crystalline insulating phase [5,38], corresponding to a primitive generator $h_{1b}^{(4)}$ [3] with topological index $\chi^{(2)} = (-1, -1, 0)$, bulk polarization

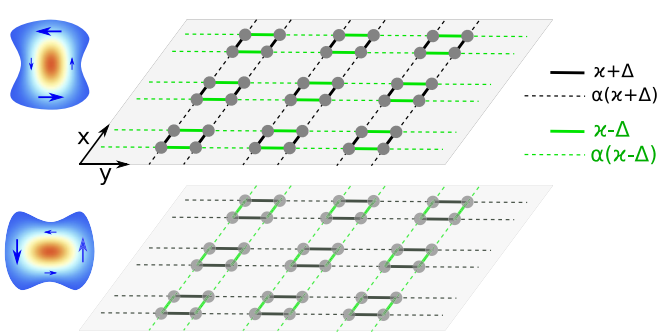

FIG. 2. Equivalent two-layer model of our system. Each layer corresponds to the anisotropic 2D SSH model with the couplings indicated in the legend for the $s \pm d$ hybrid orbitals with the field profiles depicted schematically on the left of each layer.

$P = (1/2; 1/2)$, zero bulk quadrupole moment, and alternating corner charges $\pm e/2$ at half filling [4]. These corner charges are quantized by the two commuting reflection symmetries M_x and M_y [5,38].

Thus, in the limiting case $\kappa = \gamma$ our model reduces to a pair of two noninteracting anisotropic 2D SSH layers, one rotated by 90° with respect to another (Fig. 2), which corresponds to the direct sum $h^{(4)}_{1b} \bigoplus h^{(4)}_{1b}$ of the primitive generators. The index theorem [3] then implies that the topological index of our model is the sum of indices of its primitive generators, $\chi^{(2)} = (-1, -1, 0) + (-1, -1, 0) = (-2, -2, 0)$, and the corner charge is also summed, $Q_{\text{corner}} = 2 \times e/2 = e$. Because of the pseudospin degree of freedom, integer corner charge is observable and gives rise to the pair of degenerate corner states with the distinct pseudospins, i.e., different phase shifts between s and d orbitals. The value of the corner charge is also confirmed by the direct calculation of the charge distribution at half filling where the states with $\delta k_z \leqslant 0$ are considered [Fig. 3(a)]. When $\kappa \neq \gamma$, the two anisotropic 2D SSH layers couple [35]. However, as long as the interlayer coupling does not close the bulk gap, the topology of the whole system remains the same as in the case of noninteracting layers.

The mere fact that our model, while having trivial conventional HOTI index, is a sum of two nontrivial primitive generators for opposite pseudospins allows for its further interpretation as a higher-order spin Hall insulator, and its topology is defined by the bulk polarization and corner charge for the individual pseudospin block in the limiting case of two rotated decoupled layers. Such interpretation also aligns with the physics of quantum spin Hall effect [31,39] characterized by vanishing Chern number, but nonzero and opposite Chern numbers for the two decoupled spin subsystems. Finally, the role of inversion symmetry which relates two spins in QSHE is played in our model by C_4 symmetry as seen from Fig. 2.

Corner and edge states. The higher-order topology of the system manifests itself when both constituent anisotropic 2D SSH layers are in their HOTI phases, Figs. 3(b) and 3(c). The topological corner states appear in the middle of the bulk gap with a typical field distribution shown in Fig. 3(c). To distinguish the modes by their localization, we calculate the two-mode generalization of the inverse participation ratio

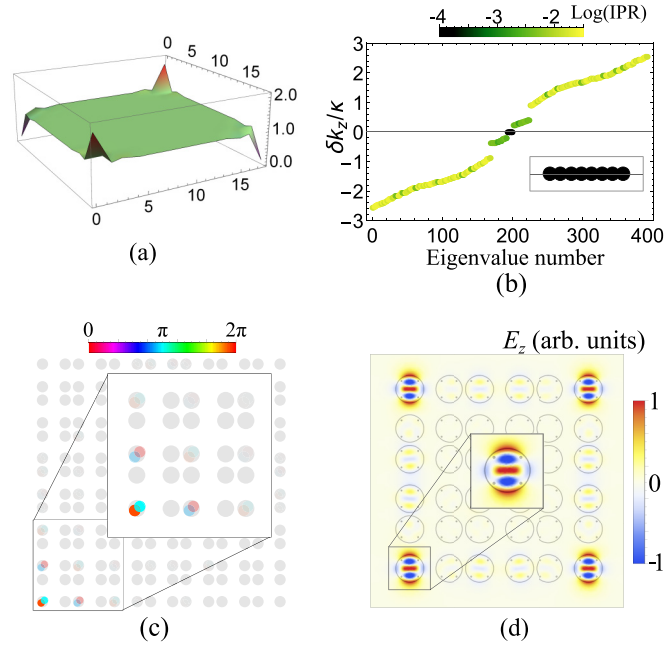

FIG. 3. (a) Charge distribution at half filling calculated for the finite lattice 14×14 sites with the same parameters as in Fig. 1. Corner charges $Q_{\text{corner}} = \pm 1$ are obtained by the summation over several sites nearest to the corner. In this calculation, on-site energies of the diagonal sites at each unit cell were set to small $\delta = \pm 10^{-2}\kappa$ as proposed in Ref. [5]. (b) Spectrum of the same finite lattice. The logarithm of inverse participation ratio is color-coded. Zoomed area shows 8-fold degenerate midgap corner states. (c) Real-space profile for one of the corner modes. Two circles in each waveguide indicate the amplitudes of the two modes, and the phase is color-coded. (d) The map of longitudinal component E_z of electric field for the corner states with propagation constants 245 rad/m obtained from the full-wave numerical simulations. Each waveguide [35] hosts TM_{02} and HE_{22} degenerate modes, and has radius 1.26 cm and permittivity $\varepsilon = 9.9$ corresponding to commercially available ceramic aluminium oxide. The center-to-center nearest-neighbor distance in expanded unit cell is 3.6 cm, and periods in x and y directions are 6.44 cm. The calculations are performed for a fixed frequency $f = 8.83$ GHz using COMSOL Multiphysics software package.

(IPR) [40]

$$\mathfrak{I} = \frac{\sum_{m,n}(|u_{mn}|^2 + |v_{mn}|^2)^2}{\sum_{m,n}(|u_{mn}|^2 + |v_{mn}|^2)}. \tag{4}$$

For different types of states, IPR shows different scaling with the size of the system N: $\mathfrak{I} \propto 1/N$ for the bulk states, $\mathfrak{I} \propto 1/\sqrt{N}$ for edge states, and $\mathfrak{I} \propto 1$ for corner states [41,42]. Indeed, we recognize three different types of scaling inspecting $\ln(\mathfrak{I})$, which is color-coded in panel (b) of Fig. 3.

Furthermore, the corner states are pinned to zero energy by the generalized chiral (sublattice) symmetry [43] which ensures that the spectrum is symmetric [35]. The localization length of the corner states measured in number of sites turns out to be $\lambda_{\text{loc}} = 1/|\ln \alpha|$, as in the one-dimensional SSH model [25,35]. Note that these corner states are not the

simultaneous end states of the SSH columns and rows (uncoupled at $\kappa = \gamma = \Delta$) since they host orthogonal orbital states.

To assess the robustness of predicted states, we also consider the effect of imperfect mode degeneracy and disorder in the couplings on the corner states. We find that the topology remains intact until the critical mode detuning which closes the bulk gap: $\delta k_c = 2(1-\alpha)\min(\gamma, \kappa)$, which is of the same order of magnitude as the couplings themselves [35]. Similarly, zero-energy corner states survive the general Hermitian disorder and retain their near-zero energy until they mix with the bulk states upon critical value of disorder comparable to the couplings [35].

In the limit $\Delta = \kappa$, the edge states shown in light green in Fig. 3(b) can be viewed as combinations of $2N$ edge states of uncoupled columns/rows with up/down orbital pseudospins, respectively, and thus inherit their topological properties directly from the one-dimensional SSH model. In particular, they are described by the same topological $\mathbb{Z}_2$ invariant (or Zak's phase) and appear at the edges connected to the bulk via the weak link. We note that while the SSH-like edge states in our model are different from the dispersive edge states in single-mode 2D SSH models [26,27,38,44,45], they are also protected by the nontrivial $\mathbb{Z}_2$ invariant along specific directions of the lattice, and have zero Chern number [46].

To confirm the predicted physics, we perform full-wave numerical simulations in microwaves, starting from a single waveguide with degenerate TM_{02} and HE_{22} modes [35]. Despite the presence of the rotated HE_{22} modes which do not interact with the modes of interest and spectrally close orbital f modes, our proposed $s-d$ model succeeds in capturing the topology of the system, and we indeed observe midgap corner states with the same propagation constant as that of the two degenerate orbitals. The calculated field profile of the corner mode is depicted in Fig. 3(d). The map of the longitudinal component E_z of electric field, which is responsible for the interorbital coupling of the chosen modes, clearly shows $s+d$ hybridized modes tightly localized at the corners. Another four $s-d$ hybrid corner states not shown here are just 90°-rotated copies of the modes shown in Fig. 3(d).

Fu-Kane-type pseudospin pump. To probe the predicted higher-order pseudospin Hall phase, we consider a Fu-Kane-like 2D adiabatic pseudospin pump. Similarly to the original proposal [47], we start from a homogeneous $s-d$ hybridized lattice and then add adiabatic out-of-phase modulation of the couplings and on-site mode detuning and examine the evolution of the eigenvalues with modulation time t. An example of such evolution of the instantaneous spectrum is shown in Fig. 4, where we observe the crossing of the four pseudospin-polarized bands of higher-order states localized at the two opposite corners. Note that pumping between other pairs of corners is also attainable for the different modulation choices. Thus, during one modulation period T, a quantized pseudospin of magnitude 2 is pumped across the diagonal.

Additionally, by establishing the analogy between modulation time t and k_z in a hypothetical 3D model, such higher-order spin pump is mapped onto the 3D weak higher-order topological insulator with pseudospin-polarized *hinge*

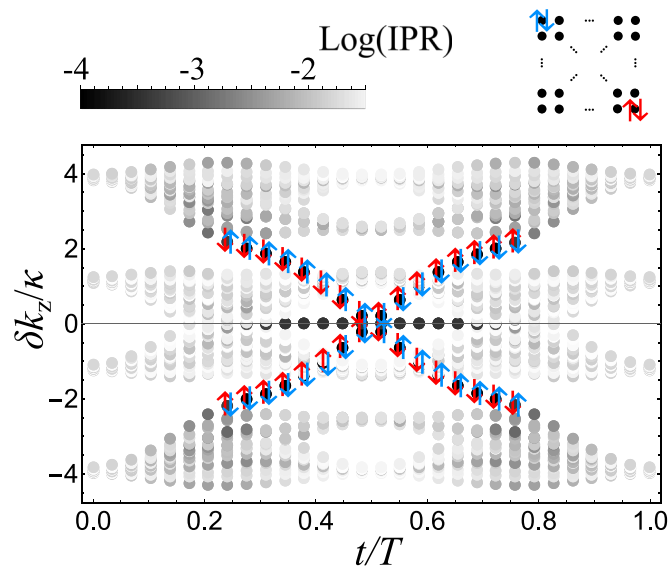

FIG. 4. Spectrum of the Fu-Kane-like 2D pseudospin pump based on $s-d$ hybridized 50×50 sites lattice versus modulation time. Arrows show the sign of the average pseudospin for the corner-localized states [35]. Color of the arrows encodes the position of the corner mode as illustrated in inset.

modes, which gives another perspective on the higher-order spin Hall terminology for our $s-d$ hybridized model. Moreover, all necessary adiabatic modulations during the pumping cycle could be readily realized in the same photonic platform of coupled waveguides [48]. In particular, the modulation of mode detuning could be realized via adiabatic change of waveguide cross section with propagation coordinate z, while the modulation of couplings could be achieved by the adiabatic bending of waveguides. The realization of such higher-order pseudospin pump is of interest on its own as an example of a higher-order pump which transfers only pseudospin (orbital angular momentum), but not charge (field amplitude).

Discussion and conclusions. In summary, we have demonstrated, both analytically and numerically, that higher-order topological states can be tailored in waveguide lattices by utilizing the interference of accidentally degenerate on-site orbital modes combined with the suitable lattice symmetry. As we prove, the combination of these mechanisms gives access to the unconventional types of topology when the net bulk dipole and quadrupole polarizations vanish while having nonzero value for the fixed pseudospin.

Our calculations show that the proposed higher-order spin-Hall system can be readily realized for the arrays of evanescently coupled microwave waveguides. We anticipate, however, that the discussed physics can be also brought to the optical range by utilizing the arrays of laser-written waveguides which have recently been shown to exhibit sizable interorbital coupling [49]. We believe that owing to the versatility and high tunability of photonic platforms, many more models and higher-order topological phases are yet to be discovered on this route.

In a broader perspective, the discussed physics is also applicable to bipartite cold-atom lattices [16] and

condensed matter systems [50]. We envision that our ideas of mode interference can be applied to engineer higher-order topology in three spatial dimensions benefiting from the multipole classification and symmetry analysis of the eigenmodes in electromagnetic resonators [51] combined with the knowledge of generalized Kerker effects [30].

Note added. Recently we became aware of a complementary work Ref. [52] which introduces the concept of spin HOTI using an alternative platform of microwave bianisotropic metamaterials. In that case, instead of *s* and *d* orbital modes the degeneracy of TE and TM polarizations is engineered.

Acknowledgments. We acknowledge Roman Savelev and Daria Smirnova for valuable discussions. Theoretical models were supported by the Russian Science Foundation (Grant No. 21-72-10107); numerical simulations were supported by the Priority 2030 Federal Academic Leadership Program. The authors acknowledge partial support by an RPMA grant of the School of Physics and Engineering of ITMO University.

[1] F. Schindler, A. M. Cook, M. G. Vergniory, Z. Wang, S. S. P. Parkin, B. A. Bernevig, and T. Neupert, Higher-order topological insulators, Sci. Adv. **4**, eaat0346 (2018).

[2] B. Xie, H.-X. Wang, X. Zhang, P. Zhan, J.-H. Jiang, M. Lu, and Y. Chen, Higher-order band topology, Nat. Rev. Phys. **3**, 520 (2021).

[3] W. A. Benalcazar, T. Li, and T. L. Hughes, Quantization of fractional corner charge in C_n-symmetric higher-order topological crystalline insulators, Phys. Rev. B **99**, 245151 (2019).

[4] W. A. Benalcazar, B. A. Bernevig, and T. L. Hughes, Quantized electric multipole insulators, Science **357**, 61 (2017).

[5] W. A. Benalcazar, B. A. Bernevig, and T. L. Hughes, Electric multipole moments, topological multipole moment pumping, and chiral hinge states in crystalline insulators, Phys. Rev. B **96**, 245115 (2017).

[6] F. Schindler, M. Brzezińska, W. A. Benalcazar, M. Iraola, A. Bouhon, S. S. Tsirkin, M. G. Vergniory, and T. Neupert, Fractional corner charges in spin-orbit coupled crystals, Phys. Rev. Research **1**, 033074 (2019).

[7] L.-H. Wu and X. Hu, Scheme for Achieving a Topological Photonic Crystal by Using Dielectric Material, Phys. Rev. Lett. **114**, 223901 (2015).

[8] J. Noh, W. A. Benalcazar, S. Huang, M. J. Collins, K. P. Chen, T. L. Hughes, and M. C. Rechtsman, Topological protection of photonic mid-gap defect modes, Nat. Photonics **12**, 408 (2018).

[9] C. W. Peterson, W. A. Benalcazar, T. L. Hughes, and G. Bahl, A quantized microwave quadrupole insulator with topologically protected corner states, Nature (London) **555**, 346 (2018).

[10] S. Mittal, V. V. Orre, G. Zhu, M. A. Gorlach, A. Poddubny, and M. Hafezi, Photonic quadrupole topological phases, Nat. Photonics **13**, 692 (2019).

[11] A. E. Hassan, F. K. Kunst, A. Moritz, G. Andler, E. J. Bergholtz, and M. Bourennane, Corner states of light in photonic waveguides, Nat. Photonics **13**, 697 (2019).

[12] X. Huang, Y. Lai, Z. H. Hang, H. Zheng, and C. T. Chan, Dirac cones induced by accidental degeneracy in photonic crystals and zero-refractive-index materials, Nat. Mater. **10**, 582 (2011).

[13] K. Sakoda, Proof of the universality of mode symmetries in creating photonic Dirac cones, Opt. Express **20**, 25181 (2012).

[14] R. S. Savelev and M. A. Gorlach, Topological states in arrays of optical waveguides engineered via mode interference, Phys. Rev. B **102**, 161112(R) (2020).

[15] G. Cáceres-Aravena, L. E. F. Foa Torres, and R. A. Vicencio, Topological and flat-band states induced by hybridized linear interactions in one-dimensional photonic lattices, Phys. Rev. A **102**, 023505 (2020).

[16] X. Li and W. V. Liu, Physics of higher orbital bands in optical lattices: A review, Rep. Prog. Phys. **79**, 116401 (2016).

[17] X. Li, E. Zhao, and W. Vincent Liu, Topological states in a ladder-like optical lattice containing ultracold atoms in higher orbital bands, Nat. Commun. **4**, 1523 (2013).

[18] G. Pelegrí, A. M. Marques, R. G. Dias, A. J. Daley, J. Mompart, and V. Ahufinger, Topological edge states and Aharanov-Bohm caging with ultracold atoms carrying orbital angular momentum, Phys. Rev. A **99**, 023613 (2019).

[19] S. Yin, J. E. Baarsma, M. O. J. Heikkinen, J.-P. Martikainen, and P. Törmä, Superfluid phases of fermions with hybridized *s* and *p* orbitals, Phys. Rev. A **92**, 053616 (2015).

[20] C. Wu, D. Bergman, L. Balents, and S. Das Sarma, Flat Bands and Wigner Crystallization in the Honeycomb Optical Lattice, Phys. Rev. Lett. **99**, 070401 (2007).

[21] A. Poddubny, A. Miroshnichenko, A. Slobozhanyuk, and Y. Kivshar, Topological Majorana states in zigzag chains of plasmonic nanoparticles, ACS Photonics **1**, 101 (2014).

[22] T. Jacqmin, I. Carusotto, I. Sagnes, M. Abbarchi, D. D. Solnyshkov, G. Malpuech, E. Galopin, A. Lemaître, J. Bloch, and A. Amo, Direct Observation of Dirac Cones and a Flatband in a Honeycomb Lattice for Polaritons, Phys. Rev. Lett. **112**, 116402 (2014).

[23] M. Milićević, T. Ozawa, G. Montambaux, I. Carusotto, E. Galopin, A. Lemaître, L. Le Gratiet, I. Sagnes, J. Bloch, and A. Amo, Orbital Edge States in a Photonic Honeycomb Lattice, Phys. Rev. Lett. **118**, 107403 (2017).

[24] M. Milićević, G. Montambaux, T. Ozawa, O. Jamadi, B. Real, I. Sagnes, A. Lemaître, L. Le Gratiet, A. Harouri, J. Bloch, and A. Amo, Type-III and Tilted Dirac Cones Emerging from Flat Bands in Photonic Orbital Graphene, Phys. Rev. X **9**, 031010 (2019).

[25] W. P. Su, J. R. Schrieffer, and A. J. Heeger, Solitons in Polyacetylene, Phys. Rev. Lett. **42**, 1698 (1979).

[26] F. Liu, H.-Y. Deng, and K. Wakabayashi, Topological photonic crystals with zero Berry curvature, Phys. Rev. B **97**, 035442 (2018).

[27] F. Liu and K. Wakabayashi, Novel Topological Phase with a Zero Berry Curvature, Phys. Rev. Lett. **118**, 076803 (2017).

[28] G. Pelegrí, A. M. Marques, V. Ahufinger, J. Mompart, and R. G. Dias, Second-order topological corner states with ultracold atoms carrying orbital angular momentum in optical lattices, Phys. Rev. B **100**, 205109 (2019).

[29] R. S. Savelev, D. F. Kornovan, V. V. Yaroshenko, and M. I. Petrov, Analogue of the Kerker effect for localized modes of discrete high-index dielectric nanowaveguides, J. Appl. Phys. **125**, 123104 (2019).

[30] W. Liu and Y. S. Kivshar, Generalized Kerker effects in nanophotonics and meta-optics, Opt. Express **26**, 13085 (2018).

[31] C. L. Kane and E. J. Mele, Z_2 Topological Order and the Quantum Spin Hall Effect, Phys. Rev. Lett. **95**, 146802 (2005).

[32] B. J. Wieder, Z. Wang, J. Cano, X. Dai, L. M. Schoop, B. Bradlyn, and B. A. Bernevig, Strong and fragile topological Dirac semimetals with higher-order Fermi arcs, Nat. Commun. **11**, 627 (2020).

[33] B. Xie, G. Su, H.-F. Wang, F. Liu, L. Hu, S.-Y. Yu, P. Zhan, M.-H. Lu, Z. Wang, and Y.-F. Chen, Higher-order quantum spin Hall effect in a photonic crystal, Nat. Commun. **11**, 3768 (2020).

[34] Z.-R. Liu, L.-H. Hu, C.-Z. Chen, B. Zhou, and D.-H. Xu, Topological excitonic corner states and nodal phase in bilayer quantum spin Hall insulators, Phys. Rev. B **103**, L201115 (2021).

[35] See Supplemental Material at http://link.aps.org/supplemental/10.1103/PhysRevB.105.205117 for details of the coupled-mode equations, generalized chiral symmetry and commuting mirror symmetries, equivalence to the two-layer model, symmetry indicators and the topological index, localization of the corner states, the effect of imperfect mode degeneracy, disorder and next-nearest-neighbor couplings on the system topology and the existence of the corner states, the realistic design at microwave frequencies, and the construction of a 2D Fu-Kane pseudospin pump based on our $s-d$ hybridized model, which includes Refs. [3–5,14,25,38,43,47,48,53–56].

[36] F. Lederer, G. I. Stegeman, D. N. Christodoulides, G. Assanto, M. Segev, and Y. Silberberg, Discrete solitons in optics, Phys. Rep. **463**, 1 (2008).

[37] M. C. Rechtsman, J. M. Zeuner, Y. Plotnik, Y. Lumer, D. Podolsky, F. Dreisow, S. Nolte, M. Segev, and A. Szameit, Photonic Floquet topological insulators, Nature (London) **496**, 196 (2013).

[38] B.-Y. Xie, H.-F. Wang, H.-X. Wang, X.-Y. Zhu, J.-H. Jiang, M.-H. Lu, and Y.-F. Chen, Second-order photonic topological insulator with corner states, Phys. Rev. B **98**, 205147 (2018).

[39] T. Ozawa, H. M. Price, A. Amo, N. Goldman, M. Hafezi, L. Lu, M. C. Rechtsman, D. Schuster, J. Simon, O. Zilberberg, and I. Carusotto, Topological photonics, Rev. Mod. Phys. **91**, 015006 (2019).

[40] D. Thouless, Electrons in disordered systems and the theory of localization, Phys. Rep. **13**, 93 (1974).

[41] N. A. Olekhno, A. D. Rozenblit, V. I. Kachin, A. A. Dmitriev, O. I. Burmistrov, P. S. Seregin, D. V. Zhirihin, and M. A. Gorlach, Experimental realization of topological corner states in long-range-coupled electrical circuits, Phys. Rev. B **105**, L081107 (2022).

[42] V. I. Kachin and M. A. Gorlach, Three-Dimensional Higher-Order Topological Insulator Protected by Cubic Symmetry, Phys. Rev. Appl. **16**, 024032 (2021).

[43] X. Ni, M. Weiner, A. Alù, and A. B. Khanikaev, Observation of higher-order topological acoustic states protected by generalized chiral symmetry, Nat. Mater. **18**, 113 (2019).

[44] X.-D. Chen, W.-M. Deng, F.-L. Shi, F.-L. Zhao, M. Chen, and J.-W. Dong, Direct Observation of Corner States in Second-Order Topological Photonic Crystal Slabs, Phys. Rev. Lett. **122**, 233902 (2019).

[45] L.-Y. Zheng, V. Achilleos, O. Richoux, G. Theocharis, and V. Pagneux, Observation of Edge Waves in a Two-Dimensional Su-Schrieffer-Heeger Acoustic Network, Phys. Rev. Appl. **12**, 034014 (2019).

[46] A. M. Marques and R. G. Dias, Topological bound states in interacting Su-Schrieffer-Heeger rings, J. Phys.: Condens. Matter **30**, 305601 (2018).

[47] L. Fu and C. L. Kane, Time reversal polarization and a Z_2 adiabatic spin pump, Phys. Rev. B **74**, 195312 (2006).

[48] O. Zilberberg, S. Huang, J. Guglielmon, M. Wang, K. P. Chen, Y. E. Kraus, and M. C. Rechtsman, Photonic topological boundary pumping as a probe of 4D quantum Hall physics, Nature (London) **553**, 59 (2018).

[49] D. Guzmán-Silva, G. Cáceres-Aravena, and R. A. Vicencio, Experimental Observation of Interorbital Coupling, Phys. Rev. Lett. **127**, 066601 (2021).

[50] M. R. Slot, S. N. Kempkes, E. J. Knol, W. M. J. van Weerdenburg, J. J. van den Broeke, D. Wegner, D. Vanmaekelbergh, A. A. Khajetoorians, C. Morais Smith, and I. Swart, *p*-Band Engineering in Artificial Electronic Lattices, Phys. Rev. X **9**, 011009 (2019).

[51] S. Gladyshev, K. Frizyuk, and A. Bogdanov, Symmetry analysis and multipole classification of eigenmodes in electromagnetic resonators for engineering their optical properties, Phys. Rev. B **102**, 075103 (2020).

[52] R. Gladstein Gladstone, M. Jung, and G. Shvets, Spin-Polarized Fractional Corner Charges and Their Photonic Realization, Phys. Rev. Lett. **128**, 026801 (2022).

[53] S.-Q. Shen, *Topological Insulators: Dirac Equation in Condensed Matter* (Springer, Heidelberg, 2013).

[54] M. Lohse, C. Schweizer, O. Zilberberg, M. Aidelsburger, and I. Bloch, A Thouless quantum pump with ultracold bosonic atoms in an optical superlattice, Nat. Phys. **12**, 350 (2016).

[55] S. Nakajima, T. Tomita, S. Taie, T. Ichinose, H. Ozawa, L. Wang, M. Troyer, and Y. Takahashi, Topological Thouless pumping of ultracold fermions, Nat. Phys. **12**, 296 (2016).

[56] M. Lohse, C. Schweizer, H. M. Price, O. Zilberberg, I. Bloch, L. Wang, M. Troyer, and Y. Takahashi, Exploring 4D quantum Hall physics with a 2D topological charge pump, Nature (London) **553**, 55 (2018).